Optik 127 (2016) 2396–2400

Contents lists available at ScienceDirect

Optik

journal homepage: www.elsevier.de/ijleo

Spherical mirror testing by phase retrieval wavefront sensor

Xinxue Ma*, Jianli Wang

Changchun Institute of Optics, Fine Mechanics and Physics, Chinese Academy of Sciences, Changchun 130033, China

ARTICLE INFO

Article history:
Received 23 October 2014
Accepted 9 September 2015

Keywords:
Phase retrieval
Wavefront sensor
Spherical mirror
Zernike polynomial
Aberration

ABSTRACT

In order to verify the estimated wavefront ability of the phase retrieval wavefront sensor (PRWS), a measured spherical mirror of experiment platform was set up with the method of PRWS. PRWS technology is based on the focal plane image information wavefront solver in the focal plane wavefront measured technology, whose principle is sampling a number of the given defocus images; get the wavefront phase information by solving the optical system wavefront with Fourier optical diffractive theory and mathematics optimization. In order to validate the veracity of PRWS, both the PRWS measurement results and ZYGO interferometer measurement results were compared; experimental results demonstrate that agreement is obtained among the errors distribution, PV value and RMS value of ZYGO interferometer, so PRWS technology can effectively estimate the aberrations of spherical mirror.

1. Introduction

In the machining processing of large-scale optics mirror, in situ real-time estimation and alignment with the use of the optical system during dynamic measurement of wave aberrations are difficult to accomplish for the present tradition optical inspection equipment [1–3]. In order to control the optical quality of the telescope, we need a simple and with high-accuracy method. This article proposed phase retrieval wavefront sensor (PRWS) technology [4–8] based on the focal plane image information wavefront solver in the focal plane estimated wavefront technology, whose principle is given by sampling a number of the defocus images [9–14]; solve the optical system wavefront by Fourier optical methods. System hardware is simple, free from the environment (especially the vibration) influence of optical components and systems for dynamic estimation, real-time display of measurements [15], which has good application prospects in the field of the optical processing, system alignment, active optics, adapt optics and others.

In order to verify the estimated wavefront ability of PRWS, this paper set up a measured spherical mirror of experiment platform with the method of PRWS based on phase retrieval (PR) theory research and experimental verification. This paper compared PRWS measurement results with ZYGO interferometer [16–22] measurement results, experimental results demonstrate that agreement is obtained among the errors distribution, PV value and RMS value of ZYGO interferometer, so using PRWS technology can effectively test the spherical mirror aberration, which illustrates the feasibility and accuracy of PRWS measurement methods.

This paper is organized as follows: the theory of PRWS is presented in Section 2, the design of experiment in Section 3 and the summary in Section 4.

2. The principles of PRWS

Phase retrieval (PR) system is the wavefront detector of a focal plane waves; a laser spot light on the object plane is a target designated from the focal plane image acquisition, use the acquired image, the defocus of the corresponding image, known pupil size and shape to reverse solve the aberration of the optical system [23]. The structure of the PR system is shown in Fig. 1.

Assuming that the aperture of a measured optical system is D, the focal length is Z, the center wavelength of the laser light source is λ, whose pupil constraint function is $\left|f(x)\right|$, the generalized pupil function for focus plane is

$$f(x) = \left|f(x)\right| \exp[\mathrm{i}\theta(x)], \tag{1}$$

where θ is wavefront distortion and can be obtained with Zernike polynomial fitting: $\theta(x) = \sum_n \alpha_n Z_n(x)$, the real number α_n represents the first *nth* terms of polynomial coefficients, Z_n indicates the first *nth* terms of Zernike polynomials basement.

For linear optical system, when the generalized pupil $f(x)$ whose defocus is δ in the plane, the impulse response function $F(u)$ is

$$F(u) = \left|F(u)\right| \exp[\mathrm{i}\psi(u)] = \mathcal{F}\left\{f(x)\exp[\varepsilon(x,\delta)]\right\}, \tag{2}$$

* Corresponding author. Tel.: +0431-86708872; fax: +0431-86708872.
E-mail address: xinxuema@hotmail.com (X. Ma).

http://dx.doi.org/10.1016/j.ijleo.2015.09.159
0030-4026/

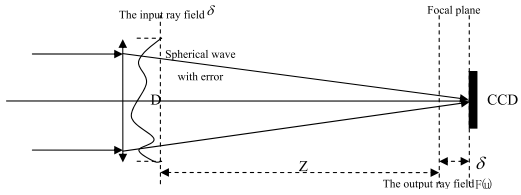

Fig. 1. Schematic of optical path of PR.

where x is the coordinates of the pupil domain, u is the coordinates of the image domain, both of them are two-dimensional vector field coordinates. ψ is the phase part of the impulse response, $\mathcal{F}$ is two-dimensional Fourier transform, $\varepsilon(x, \delta)$ is wavefront aberration caused by defocus δ in the position x.

For a PR system, $|f(x)|$ of Eq. (1) is the priori conditions of a known optical system, corresponds to the size and shape of the pupil. $|F(u)|^2$ is the image collected by CCD where the defocus is δ. Therefore, the purpose that we estimate wavefront by PR is to get α_n by the above known quantity. So formal description of the problem for: $|f(x)|$, δ_1, $|F_1(u)|^2$, δ_2, $|F_2(u)|^2$, ..., δ_M, $|F_M(u)|^2$ are known. Image acquisition distance from the focal plane at δ_1, δ_2, ..., δ_M, respectively, is $|F_1(u)|^2$, $|F_2(u)|^2$, ..., $|F_M(u)|^2$.

The objective function and the partial derivative of PR objective function with respect to α_n, respectively, is formulas (3) and (4)

$$B_k = E_{Fk}^2 = N^{-2}\sum_{m=1}^{M}\sum_{u}[|G_{m,k}(u)| - |F(u)|]^2, \tag{3}$$

$$\partial_{a_n} B_k = -2\sum_{m}\sum_{x} |f(x)|\,|g'_{m,k}(x)| \sin[\theta'_{m,k}(x) - \theta_{m,k}(x)]Z_n(x). \tag{4}$$

With the objective function (3) and its impact on the Zernike coefficient derivative (4), we can use the mathematical optimization algorithm to solve various Zernike wavefront coefficient values, here we use LBFGS algorithm that the phase diversity (PD) [24–30] experiment has been able to solve.

3. The design of the experiments

3.1. Experimental theory and components

The schematic diagram of PRWS is shown in Fig. 2. Gaussian beam emitted from the laser through the pinhole into a spherical wave, passes through the lens 2 into a parallel light, the light projects in the prism through the prism is divided into two parts, a part need not be considered, another part of the parallel reflects after a light through the lens 1 converge after the measured mirror, the reflected beam with phase [31–35] information (i.e. aberration), again divided into two groups by a beam splitter, one part backtrack, the other part through the converging lens 3 converged at CCD camera, which is placed on a movable platform, move along the optical axis and the angle of the camera posture fine-tuning to get the focus before and after receiving a different amount of defocus

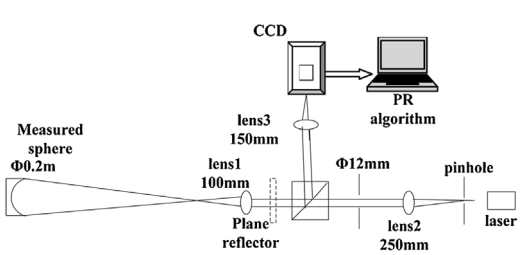

Fig. 2. Schematic diagram of PRWS.

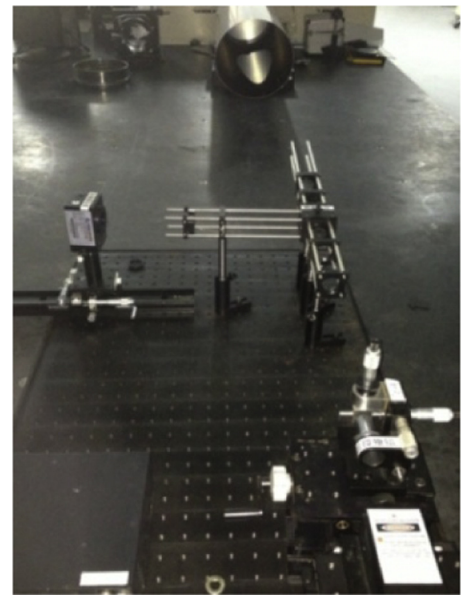

Fig. 3. The experimental system of PRWS.

images [36–39],used in realizing the estimated wavefront based on the PR. We can obtain aberration of the measured spherical mirror with the PR algorithm.

The focal length of measured spherical mirror is 0.2 m, the center wavelength is 632.5 nm, focal length of 3 in the experimental system is 0.15 m, the exit pupil caliber is 0.012 m, and the depth of focus is about 0.286 mm. In the experiment, the defocus we select is 0,±1, ±1.5, ±2 mm. Camera pixel size is 6.45 μm, each defocus position, respectively, intercept 128 × 128 pixel size of target region, the exposure time is 20 ms, the accuracy of mobile platform is ± 5 μm. The experimental optical path is shown in Fig. 3.

3.2. Experimental procedures

In the process of the entire experiment, we not only prove the estimation ability of PRWS, but also prove the accuracy of PRWS, therefore during the experimental design, in order to ensure that the position of the measured spherical mirror during the whole experiment is invariable, we need to find the good distance between spherical mirror with PRWS devices and between spherical mirror with ZYGO, respectively, based on the focal lengths of the measured spherical mirror. Then separately measure the spherical mirror with PRWS and ZYGO.

Step1: build experiment system. Firstly, fix the 0.2 m telescope as shown in Fig. 4; secondly, place the laser and the position of the pinhole as shown in Fig. 5. The requirements of laser position are: laser light and the center of the telescope mirror are coaxial. After regulating, put the microscope objective and a pinhole placed in front of the laser making the light from the pinhole in an ideal spherical wave. Lastly, reconfirm the laser, pinhole, spherical mirror are coaxial, as shown in Fig. 6.

Fig. 4. Tested telescope.

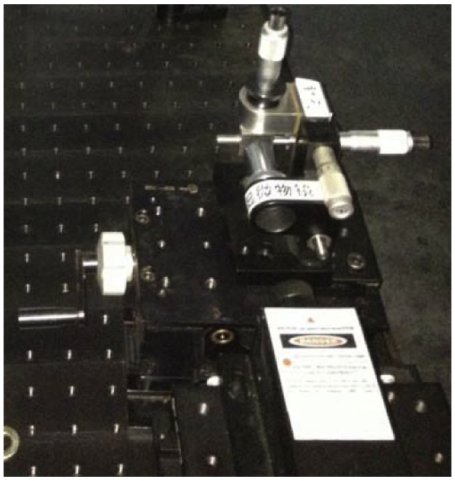

Fig. 5. laser and pinhole.

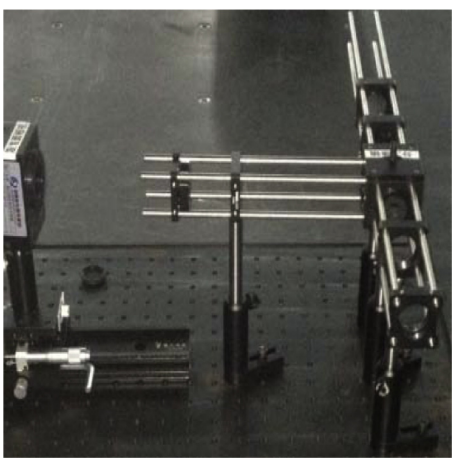

Fig. 6. Coaxial system.

Step 2: add the lens 1, and adjust the position of the lens 1 to make it to be coaxial with the laser and pinhole until the spherical wave is emitted from the pinhole through the lens 1 into parallel light;

Step 3: add the splitting prism, light bar and the lens 2 in the optical path, and make them be coaxial with the measured spherical mirror and pinhole, then according to the parallelism of the return light beam from splitter to adjust the position of the lens 2;

Step 4: adjust the position of the lens 3 and the camera to make the light beam reflect from the measured spherical light through the prism to enter into the camera;

Step 5: after adjusting the system, adjust the translation stage to make the point of light least, then record the location and use it at the position of the focal point;

Step 6: capture images with the camera at the position of the defocus distances of ± 1, ±1.5, ±2 mm;

Step 7: put the plane mirror between the lens 1 and the prism, repeat the above steps to capture images with the camera;

Step 8: dispose the images collected of the sixth and seventh steps with the PD algorithm, get the aberration of the measured spherical mirror;

Step 9: ensure that the position of the measured spherical mirror remains unchanged, use the ZYGO interferometer estimate the measured spherical mirror. Fig. 7 is a diagram of the estimation experiment with the ZYGO interferometer.

Fig. 7. The experimental system of ZYGO interferometer measurement.

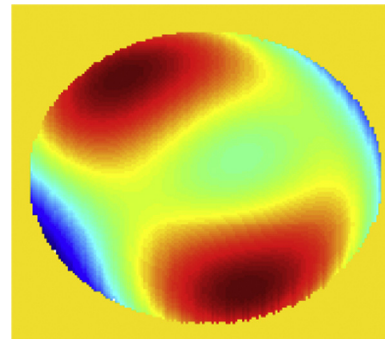

Fig. 8. Result of PRWS, RMS = 0.272λ, PV = 1.608λ

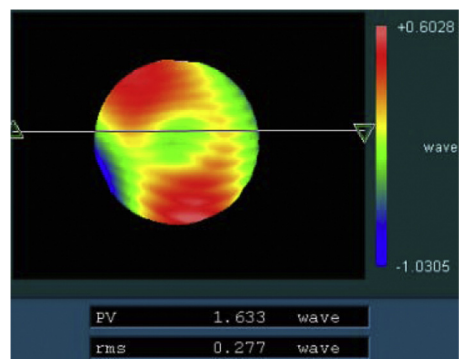

Fig. 9. Result of ZYGO interferometer, RMS = 0.277λ, PV = 1.633λ.

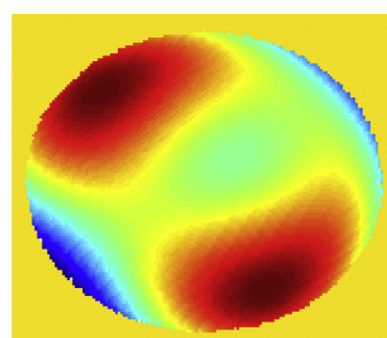

Fig. 10. Result of PRWS after rotation.

3.3. Experimental results and discussion

We dispose the collected seven images with the PR algorithm, obtain the measured result of the spherical mirror as shown in Fig. 8. The measured result with the ZYGO interferometer is shown in Fig. 9.

In order to illustrate the accuracy and viability of the PRWS better, we rotated the spherical mirror a definite degree, and then estimate the spherical mirror with steps one to nine, the obtained measurement results are shown in Figs. 10 and 11.

In order to illustrate the accuracy and repeatability of PR, we rotated the spherical mirror some degree, and then estimate the

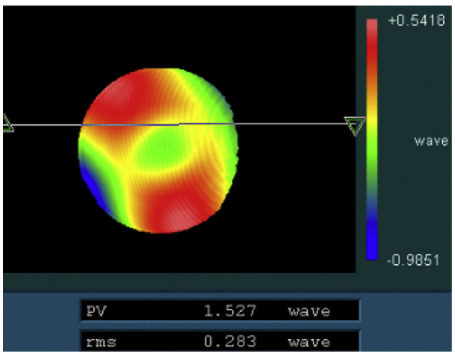

Fig. 11. Result of ZYGO interferometer after rotation, RMS = 0.280λ, PV = 1.501λ RMS = 0.283λ, PV = 1.527λ.

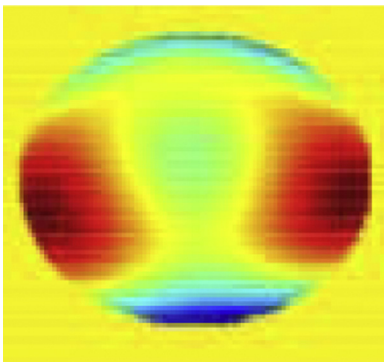

Fig. 12. Result of PR measurement after rotation, RMS = 0.271λ, PV = 1.659λ.

Table 1
Comparison of Zernike polynomials.

ITEMS	Zernike	ZYGO	PRWS
1	Piston	0	0
2	X tilt	0	0
3	Y tilt	0	0
4	Defocus	0	0
5	Ast x	-0.380	-0.372
6	Ast Y	-0.552	-0.543
7	Coma x	0.018	-0.017
8	Coma Y	0.044	0.043
9	Primary Spherical	-0.217	-0.213
10	Trefoil x	-0.013	-0.012
11	Trefoil y	0.240	0.235
12	Secondary Ast x	0.045	0.044
13	Secondary Ast y	0.028	0.027
14	Secondary coma x	-0.065	-0.063
15	Secondary coma y	-0.007	-0.006
16	Secondary Spherical	0.100	0.099
17	Tetrafoil x	0.030	0.029
18	Tetrafoil y	0.014	0.013
19	Secondary Trefoil x	-0.020	-0.019

spherical mirror with steps one to nine, the obtained measurement results are shown in Fig. 12.

In order to verify the accuracy of PRWS we compared the 19th Zernike polynomials of Figs. 10 and 11 and get the results as shown in Table 1.

From the results of Table 1, we can see that the Zernike polynomials of PRWS and ZYGO are linear relationship, which is the same as the difference RMS between PRWS and ZYGO. From the measurement result after rotating, as shown in Fig. 12, the results of estimated wavefront before and after rotation are in agreement, which verifies the repeatability and effectiveness of PRWS measurement. Seeing from Figs. 8–11, there is an agreement among the errors distribution, PV value and RMS value of ZYGO interferometer, which explains the feasibility and accuracy of the PRWS measurement methods.

4. Conclusions

This paper set up an estimation spherical mirror of experiment platform with the method of PRWS, from the contrast of the measurement results before and after rotation, which verified the PRWS measurement repeatability and effectiveness. In order to validate the veracity of PRWS, this paper compared PRWS measurement results with ZYGO interferometer measurement results, experimental results demonstrate that agreement is obtained among the errors distribution, PV value and RMS value of ZYGO interferometer, so using PRWS technology can effectively estimate the spherical mirror aberration, which explains the feasibility and accuracy of the PRWS measurement methods, which provides the feasibility to data support for our later search.

Acknowledgment

This work is supported by the National High-tech Research and Development Program (863 Program) (No. 2009AA8080603).

References

[1] B. Brown, M. Aaron, The Politics of Nature, in: J. Smith (Ed.), The Rise of Modern Genomics, 3rd edn, Wiley, New York, 2001.
[2] R. Brady Gregory, P.J.R. Fienu, Improved Optical Metrology Using Phase Retrieval [C], Optical Fabrication & Testing, Rochester, NY, 2004, pp. 10 1–103.
[3] M. Svedendahl, R. Verre, M. Käll, Refractometric biosensing based on optical phase flips in sparse and short-range-ordered nanoplasmonic layers [J], Light Sci. Appl. 3 (2014) e220.
[4] W. Osten, Some answers to new challenges in optical metrology[C], Proc. SPIE 7155 (2008), 715503-1- 715503-16.
[5] C.M. Ohara, J.A. Faust, A.E. Lowman, et al., Phase retrieval camera optical testing of the advanced mirror system demonstrator [C], SPIE 5487 (2004) 1744–1756.
[6] R.W. Gerchberg, W.O. Saxton, A practical algorithm for the determination of phase from image and diffraction phase pictures [J], Optic 35 (2) (1972) 237–246.
[7] J.R. Fienup, Phase retrieval algorithms: a comparison [J], Appl. Opt. 21 (15) (1982) 2758–2769.
[8] J.R. Fienup, J.C. Marron, T.J. Schulz, et al., Hubble space telescope characterized by using phase-retrieval algorithms [J], Appl. Opt. 32 (10) (1993) 1747–1767.
[9] H. Dean Bruce, L. Aronstein David, J.S. Smith, et al., Phase retrieval algorithm for JWST flight and testbed telescope[C], Proc. SPIE 6265 (2006) 1–17.
[10] B. Park, S.H. Yun, C.Y. Cho, Y.C. Kim, J.C. Shin, H.G. Jeon, Y.H. Huh, I. Hwang, K.Y. Baik, Y.I. Lee, H.S. Uhm, G.S. Cho, E.H. Choi, Surface Plasmon excitation in semitransparent inverted polymer photovoltaic devices and their applications as label-free optical sensors [J], Light Sci. Appl. 3 (2014) e222.
[11] T. Strudley, R. Bruck, B. Mills, O.L. Muskens, An ultrafast reconfigurable nanophotonic switch using wavefront shaping of light in a nonlinear nanomaterial [J], Light Sci. Appl. 3 (2014) e207.
[12] A.M. Flatae, M. Burresi, H. Zeng, S. Nocentini, S. Wiegele, C. Parmeggiani, H. Kalt, D. Wiersma, Optically controlled elastic microcavities [J], Light Sci. Appl. 4 (2015) e282.
[13] A.J. Devaney, R. Childlaw, On the uniqueness question in the problem of phase retrieval from intensity measurement [J], JOSA A 68 (10) (1978) 1352–1354.
[14] Z. Zhang, Z. You, D. Chu, Fundamentals of phase-only liquid crystal on silicon [J], Light Sci. Appl. 3 (2014) e213.
[15] Fu Fuxing, B. Zhang, Recovery of high frequency phase of laser beam with wavefront distortio[J], Chinese J. Lasers 38 (4) (2011) 0402009.
[16] R. Brady gregory, P.J.R. Fienu, Phase retrieval as an optical metrology tool[C] optical fabrication and testing, in: Topical Meeting of the Optical Society of America, SPIE Technical Digest, 2005, pp. 139–141.
[17] J.E. Millerd, J.C. Wyant, Simultaneous phase-shifting Fizeau interferometer [P].US Patent (2005), 20050046864.
[18] D. Leslie, Vibration-resistant phase-shifting interferometry[J], Appl. Opt. 35 (34) (1996) 6655–6662.
[19] J.H. Burge, J.C. Wyant, Applications of computer-generated holograms for interferometric measurement of large aspheric optics[C], Proc. SPIE (1995).
[20] S. Reichelt, C. Pruss, H.J. Tiziani, Absolute interferometric test of aspheres by use of twin computer- generated holograms [J], Appl. Opt. 42 (22) (2003) 4468–4479.
[21] S.L. Diedenhofen, D. Kufer, T. Lasanta, G. Konstantatos, Integrated colloidal quantum dot photodetectors with color-tunable plasmonic nanofocusing lenses [J], Light Sci. Appl. 4 (2015) e234.
[22] S. Reichelt, H.J. Tiziani, Twin-CGHs for absolute calibration in wavefront testing interferometry [J], Opt. Commun. 220 (2003) 23–32.
[23] X. Ma, J. Wang, B. Wang, Study on phase retrieval algorithm [J], Laser Infrared 42 (2) (2012) 217–221.

[24] J.L. Wang, Z.Y. Wang, B. Wang, et al., Image restoration by phase-diversity speckle [J], Opt. Precis. Eng. 19 (5) (2011) 1165–1170.
[25] B. Wang, Z.Y. Wang, J.L. Wang, et al., Phase-diverse speckle imaging with two cameras [J], Opt. Precis. Eng. 19 (6) (2011) 1384–1390.
[26] J.Y. Zhao, Z.F. Chen, B. Wang, et al., Improvement of phase diversity object function's parallelity, J. Opt. Precis. Eng. 20 (2) (2012) 431–438.
[27] B. Wang, X.X. Ma, et al., Calibration of no-common path aberration in AO system using multi-channel phase-diversity wave-front sensing [J], Opt. Precis. Eng. 21 (7) (2013) 1683–1692.
[28] Z.Y. Wang, B. Wang, Y.H. Wu, et al., Calibration of non-common path static aberrations by using phase diversity technology [J], Acta Opt. Sin. 32 (7) (2012) 0701007.
[29] J.Y. Zhao, X.X. Ma, et al., Image restoration based on real time wave-front information [J], Opt. Precis. Eng. 20 (6) (2012) 1350–1356.
[30] R.H. Byrd, P. Lu, J. Nocedal, A limited-memory algorithm for bound-constrained optimization, SIAM J. Sci. Stat. Comput. 16 (5) (1995) 1190–1208.
[31] M. Gu, H.C. Bao, X.S. Gan, N. Stokes, J.Z. Wu, Tweezing and manipulating micro- and nanoparticles by optical nonlinear endoscopy [J], Light Sci. Appl. 3 (2014) e126.
[32] N. Accanto, J.B. Nieder, L. Piatkowski, M. Castro-Lopez, F. Pastorelli, D. Brinks, N.F. van Hulst, Phase control of femtosecond pulses on the nanoscaleusing second harmonic nanoparticles[J], Light Sci. Appl. 3 (2014) e143.
[33] C.S. Liao, M.N. Slipchenko, P. Wang, J. Li, S.Y. Lee, R.A. Oglesbee, J.X. Cheng, Microsecond scale vibrational spectroscopic imaging by multiplex stimulated Raman scattering microscopy [J], Light Sci. Appl.4 (2015) e265.
[34] A.E. Cetin, A.F. Coskun, B.C. Galarreta, M. Huang, D. Herman, A. Ozcan, H. Altug, Handheld high-throughput plasmonic biosensor using computational on-chip imaging [J], Light Sci. Appl. 3 (2014) e122.
[35] X.L. Deán-Ben, R. Daniel, Adding fifth dimension to optoacoustic imaging: volumetric time-resolved spectrally enriched tomography [J], Light Sci. Appl. 3 (2014) e137.
[36] X. Chen, C. Zou, Z. Gong, C. Dong, G. Guo, F. Sun, Subdiffraction optical manipulation of the charge state of nitrogen vacancy center in diamond [J], Light Sci. Appl.4 (2015) e230.
[37] N. Tischler, I. Fernandez-Corbaton, X. Zambrana-Puyalto, A. Minovich, X. Vidal, M.L. Juan, G. Molina-Terriza, Experimental control of optical helicity in nanophotonics [J], Light Sci. Appl.3 (2014) e183.
[38] A. Polyakov, M. Melli, G. Cantarella, A. Schwartzberg, A. Weber-Bargioni, P.J. Schuck, S. Cabrini, Coupling model for an extended-range plasmonic optical transformer scanning probe [J], Light Sci. Appl. 3 (2014) e195.
[39] X. Fang, K.F. MacDonald, N.I. Zheludev, Controlling light with light using coherent metadevices:all-optical transistor, summator and invertor [J], Light Sci, Appl.4 (2015) e292.